Research Project

Parametric Study of Particle-Surface Wave Interactions: A Hydrodynamic Analog of Relativistic Quantum Dynamics

Idan Ceausu
Supervisor: Yuval Dagan
Faculty of Aerospace Engineering
Technion – Israel Institute of Technology

December 30, 2020

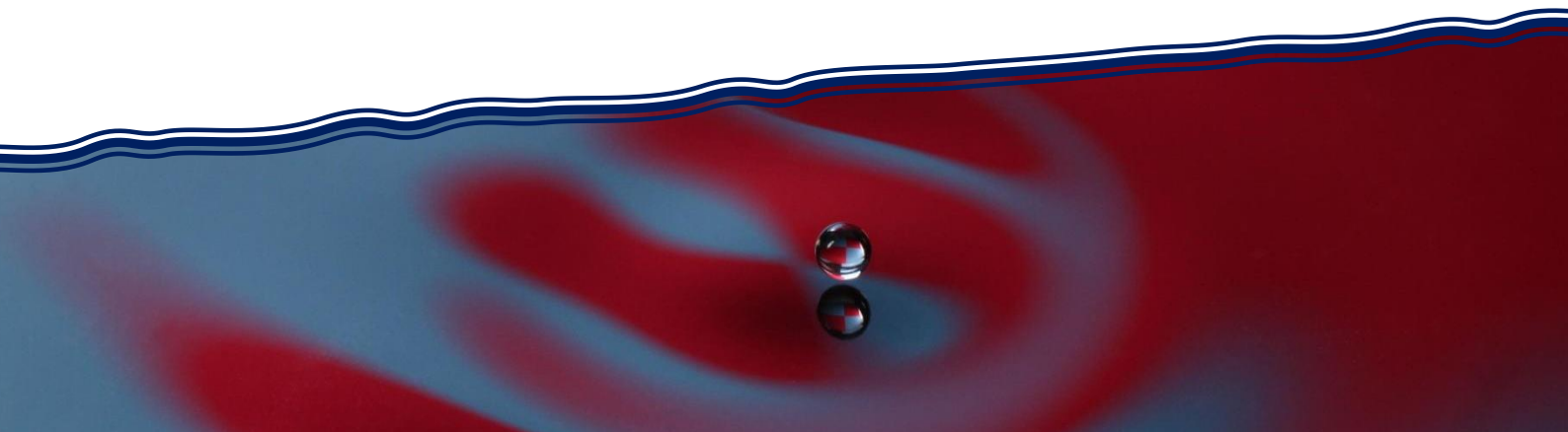

Contents

1 Introduction **2**

2 Mathematical Model **3**
2.1 The Wave Equation . . . 3
2.1.1 Quantum Physics . . . 3
2.1.2 Fluid Dynamics . . . 3
2.1.3 Generalized Pilot-Wave Equation . . . 4
2.2 The Dynamic Equation . . . 5

3 Numerical Method **6**
3.1 Finite Differences Scheme . . . 6
3.2 Spectral Method for Periodic Grids Scheme . . . 7
3.3 Sensitivity Tests for the Spectral Method . . . 8
3.4 Comparison between Finite Differences and the Spectral Method . . . 9

4 Results and Discussion **11**
4.1 Particle Dynamics and Wave-Form . . . 11
4.2 Particle Statistics and Typical Properties . . . 14

5 Conclusions and Future Research **16**

Chapter 1

Introduction

In 2005, Couder and Fort experimentally observed a phenomenon involving millimetric oil droplets bouncing over a vibrating bath of the same liquid that behaves analogously to several quantum mechanical systems-the Hydrodynamic Quantum Analog (HQA) [1–4]. In this analog, droplets interact in resonance with the quasi-monochromatic wave-field they create, which causes a self-propelling mechanism; this is possible due to a pervading air layer that prevents the droplet from coalescing into the bath. The walking droplet systems has extended the range of classical physics to include many features previously thought to be exclusively quantum, including particle diffraction [5], quantum tunneling [6–8], quantized orbits [9–11], the Zeeman Effect [12], and the quantum corral [13–16]. Besides being fascinating, bouncing droplets can be viewed as an analog of the pilot wave theory, one of many quantum mechanics interpretations, and a part of the hidden-variable theories.

Recently, Dagan and Bush developed a hydrodynamically-inspired quantum field theory (HQFT) [17, 18], a theoretical model of quantum dynamics based on the pilot-wave theory of de Broglie and insights from the walking-droplet system. According to de Broglie, particle and wave duality is manifested through a pilot wave responsible for guiding the particle. This mechanism has two sides, one that generates the pilot wave and one for the wave's guiding effect on the particle. HQFT presents a mechanism for these wave-particle interactions based on de Broglie's hypothesis and the walking droplet system. The theory describes the pilot wave using the Klein–Gordon (KG) equation with an oscillating localized disturbance, and in response, using a dynamic equation, the particles walking on the surface are propelled by a wave force proportional to the slope of the local wave field. In [17], by adding to the dynamic equation a proper Lorentz boost factor, the particle motion was forced to be relativistic so that the particle wouldn't pass the speed of light. However, in this project, we tried a different approach regarding the particle's motion and relaxed the restriction on the particle's velocity; hence, as a classical non-relativistic theory, it can describe millimetric droplets bouncing on water-waves as well as quantum particles of much smaller scales. The theoretical model comprises of two coupled equations, one for the wave-field and the second, the guiding equation for the particle motion.

A spectral method was developed here to solve the coupled particle-wave system, which is based on Discrete Fourier Transform. We also wrote a finite differences (FD) code for validation. Using convergence tests and by comparing to the FD solution, we inferred that the computational difficulty is not expressed by each of the equations separately, but by their coupling, which contains a combination of small scales and large scales of the problem.

Using our spectral simulations, we found multiple phenomena that exhibit the particle's inherent relativistic behavior, even though we relaxed the dynamic equation's restrictions that forced the particle to be relativistic. The results also provide an interesting relation between the particle trajectory and the waveform, which behaves as expected from the fundamental quantum relation $p = \hbar k$. The combination of these findings suggests new non-relativistic hydrodynamic analogs to quantum relativistic particle dynamics.

Chapter 2

Mathematical Model

The mathematical model used in the present study can be generally described by two equations, a wave equation, and a dynamic equation, from two physics fields of completely different scales: Quantum Mechanics (QM) and Fluid Dynamics. For the wave-field, we use a Klein-Gordon (KG) wave equation, which has the same form in Quantum Field Theory (QFT) for spinless particles [19] and in deep-water surface waves in hydrodynamics [20]. The second equation is a dynamic equation derived from Fluid Dynamics. The combination of both allows us to explain some fundamental aspects of quantum mechanics.

2.1 The Wave Equation

2.1.1 Quantum Physics

According to de Broglie's pilot-wave theory, the duality of particle and wave is manifested by a pilot wave responsible for guiding the particle. This mechanism has two sides, one that generates the pilot wave and one for the wave's guiding effect on the particle. Hydrodynamic quantum field theory presents the walking droplet system as a mechanism for these wave-particle interactions [17]. The theory describes the pilot wave using the Klein–Gordon (KG) equation with a localized disturbance oscillating as a droplet-particle.

The derivation of KG stems from special relativity where the relativistic energy of a free particle is described with the identity of Einstein:

$$E^2 = p^2c^2 + {m_0}^2c^4 \tag{2.1}$$

where p is the momentum, m_0 is the rest mass of the particle, and c is the speed of light. In Quantum Physics, the relations between energy and momentum to frequency and the wavenumber are defined by $\hbar$, according to de Broglie's hypothesis:

$$\begin{aligned} E &= \hbar\omega \\ p &= \hbar k \end{aligned} \tag{2.2}$$

Substituting (2.2) into (2.1), we find the dispersion relation for the KG equation,

$$\omega^2 = k^2c^2 + \frac{{m_0}^2c^4}{\hbar^2} \tag{2.3}$$

2.1.2 Fluid Dynamics

Consider a bath with a depth of H driven by vertical vibration of amplitude A and frequency $f = \omega/2\pi$. The effective gravity in the vibrating bath frame of reference is $g^*(t) = g + \gamma \sin(2\pi f t)$, where g is the gravitational

acceleration and $\gamma = A\omega^2$. At low forcing accelerations, the fluid remains quiescent in the vibrating frame. However, above a critical acceleration of amplitude γ_F, corresponding to the Faraday threshold, the flat surface becomes unstable as a field of standing Faraday waves. The waves are subharmonic, with a characteristic frequency of half the driving frequency of the vibrational forcing, $\omega_F = \omega/2$, and wavelength $\lambda_F = 2\pi/k_F$. The dispersion relation of the surface wave of this system influenced by gravity and capillary effects is [20]:

$$\omega_F^2 = tanh(k_F H)\left(\frac{\sigma k_F^3}{\rho} + g k_F\right) \tag{2.4}$$

where ρ and σ are the density and the surface tension of the fluid. Assuming the bath is deep enough, so $tanh(k_F H) \longrightarrow 1$, and all the modes of the wave decay fast except for k_F, we get by (2.4), for an almost constant wave number, monochromatic waves with dispersion relation of (2.3):

$$\omega_F^2 = |k_F|\left(\frac{\sigma}{\rho}k_F^2 + g\right) \tag{2.5}$$

Combining a bouncing droplet to the system will be treated as a periodic disturbance of the wave field, which act due to the KG equation.

2.1.3 Generalized Pilot-Wave Equation

We can now compare (2.3) to (2.5), both of them have the dispersion relation of KG, and a comparison between the different terms is described in the table:

	Quantum Physics	**Fluid Dynamics**	**Present Study**
Dispersion Relation	$\omega^2 = c^2k^2 + \frac{{m_0}^2c^4}{\hbar^2}$	$\omega_F^2 = \lvert k_F\rvert\frac{\sigma}{\rho}k_F^2 + \lvert k_F\rvert g$	$\omega^2 = c^2k^2 + \omega_n^2$
Natural Frequency	$\omega_c = \frac{m_0c^2}{\hbar}$	$\sqrt{\lvert k_F\rvert g}$	ω_n
Maximum Signaling Velocity	c	$\sqrt{\lvert k_F\rvert\frac{\sigma}{\rho}}$	c
Characteristic Wave Length	$\lambda_c = \frac{h}{m_0c}$	$2\pi\sqrt{\frac{\sigma}{\rho g}}$	λ_n

From now on, the variable ω is the frequency satisfying the dispersion relation of:

$$\omega^2 = c^2k^2 + \omega_n^2 \tag{2.6}$$

Using this dispersion relation, a general 1D Klein–Gordon equation can be written as

$$\varphi_{tt} - c^2\varphi_{xx} + \omega_n^2\varphi = 0 \tag{2.7}$$

Dagan and Bush [17] used the KG wave-field, and inspired by de Broglie's pilot-wave theory, modeled the local disturbance caused by the particle as an external force, that depends on the location of the particle:

$$\varphi_{tt} - c^2\varphi_{xx} + \omega_n^2\varphi = F(x, x_p, t) \tag{2.8}$$

For the local disturbance, we use a Gaussian function multiplied by a periodic function [17]:

$$F(x, x_p, t) = -\sin(\Omega t)\exp\left[-\frac{(x - x_p)^2}{(\frac{1}{2}\lambda_n)^2}\right] \tag{2.9}$$

The shape of the disturbance is a result of some insights from QM and the droplet system. A walking droplet undergoes a self-propelling motion through a resonant interaction with its own wave field, where a number of bounce frequencies exits. The frequency in our model was set following Schrödinger, who proposed that the particle vibration, the so-called Zitterbewegung, takes place at twice the Compton frequency, which gives rise to a vibration at $\Omega = 2\omega_n$. In our model x_p is the location of the particle, the width of the Gaussian is the extent of the particle's influence on the wave-field. The characteristic particle influence arises on the scale of the wavelength λ_n, as can be see in the Gaussian width scale. Proper normalization of the modified KG equation will allow comparison between the QM and the hydrodynamic system. By defining the reduced wavelength,

$$\lambda\!\!\!^{-}_n = \frac{\lambda_n}{2\pi} \tag{2.10}$$

and the normalized variables,

$$\tilde{\varphi} = \frac{\varphi}{\lambda\!\!\!^{-}_n} \quad \tilde{x} = \frac{x}{\lambda\!\!\!^{-}_n} \quad \tilde{t} = \omega_n t \tag{2.11}$$

and also omitting all the "Tilde", we get the normalized KG equation:

$$\varphi_{tt} - \varphi_{xx} + \varphi = F(x, x_p, t) = -\sin(2t)\exp\left[-\frac{(x - x_p)^2}{\pi^2}\right] \tag{2.12}$$

This equation describes a real pilot wave generated through a local interaction in resonance with the vibrating particle. For the sequel, we will define the time period:

$$\tau_n = \frac{2\pi}{\omega_n} \tag{2.13}$$

2.2 The Dynamic Equation

In this model, the dynamics of droplets walking on the surface of a vibrating bath in resonance with their guiding wave is based on the assumption that the vertical motion is fast relative to the horizontal so that the drop may be treated as a continuous source of waves along its path. The resulting trajectory equation describing the droplet's horizontal displacement x_p is taken from [21]:

$$m\ddot{x}_p = -D\dot{x}_p - mg\nabla h(x_p, t) \tag{2.14}$$

The droplet is propelled by a wave force proportional to the slope of the local wave field $h(x, t)$, resisted by a linear drag induced during flight and impact, and characterized by a constant drag coefficient D. Another assumption is that we are dealing with lightweight particles, so we neglect the droplet inertia: the particle simply moves in response to its pilot wavefield gradients. By rearranging the equation, we get the guiding equation:

$$\dot{x}_p = -\alpha \frac{\partial \varphi}{\partial x}\Big|_{x_p} \tag{2.15}$$

The wave field produced by prior oscillations guides the particle so that its velocity is proportional to the gradient of the wave amplitude. In [17], this equation has another term associated with the limitation of the particle velocity. The velocity is multiplied by the Lorentz boost $\gamma = 1/\sqrt{1 - (v/c)^2}$, which requires that the particle's motion in the quantum scales remains under c. However, here we relax this restricting assumption, and the guidance equation for the particles in this case is gradient-driven only. During the osculations and depending on α and the wave gradient, $\dot{x}_p$ may exceed the speed of light (or in fluid dynamics the maximum signaling speed of the wave), but as will be shown in section 5, fast oscillation beyond c will only occur on the small scales (Compton scale in QM). On average, the motion will always be at speeds lower than c.

Chapter 3

Numerical Method

A numerical scheme is derived to solve the mathematical particle-wave model as a non-linear coupled system of partial differential equations:

$$\begin{cases} \varphi_{tt} - \varphi_{xx} + \varphi = F(x, x_p, t) = -\epsilon \sin(2t) \exp\left[-\frac{(x - x_p^2)}{\pi^2} \right], \quad -L < x < L, \quad t > 0 \\ \dot{x}_p = -\alpha \varphi_x \Big|_{x_p} \end{cases} \tag{3.1}$$

We assume that the wave will vanish at the domain edges far away from the particle motion, so the boundary conditions are:

$$\varphi(\pm L, t) = 0 \tag{3.2}$$

Initial Conditions:

$$\varphi(x, 0) = 0, \quad \varphi_t(x, 0) = 0, \quad x_p(t = 0) = 0 \tag{3.3}$$

In this study, we will explore the different numerical schemes, Finite Difference (FD) and a spectral method, for a solution of the coupled non-linear system. Comparing the results from both schemes will also allow the validation of our code.

3.1 Finite Differences Scheme

The second derivative of a function can be approximated, by the central difference of second order:

$$f''(x) \approx \frac{f(x + \Delta x) - 2f(x) + f(x - \Delta x)}{(\Delta x)^2} \tag{3.4}$$

Thus, for the Klein–Gordon equation:

$$\frac{\varphi(x, t + \Delta t) - 2\varphi(x, t) + \varphi(x, t - \Delta t)}{(\Delta t)^2} - \frac{\varphi(x + \Delta x, t) - 2\varphi(x, t) + \varphi(x - \Delta x, t)}{(\Delta x)^2} + \varphi(x, t) = F(x, x_p, t) \tag{3.5}$$

and one can get the update for future time term:

$$\varphi(x, t + \Delta t) = r^2[\varphi(x + \Delta x, t) - \varphi(x - \Delta x, t)] + [-2r^2 - b^2 + 2]\varphi(x, t) - \varphi(x, t - \Delta t) + b^2 F(x, x_p, t) \tag{3.6}$$

where $r = \frac{\Delta t}{\Delta x}$ and $b = \Delta t$, Δx is the spatial interval and Δt is the temporal interval.
Now that we have the wave function all over the domain, for the next loop we need to find the updated particle

location x_p. The equation of motion for the particle will be solved by interpolation of the gradient

$$\varphi_x \approx \frac{\varphi(x+\Delta x,t)-\varphi(x-\Delta x,t)}{2\Delta x} \tag{3.7}$$

at the location of the particle:

$$x_p(t+\Delta t) = x_p(t) - \alpha \frac{\partial \varphi}{\partial x}\Big|_{x_p(t)} \Delta t \tag{3.8}$$

3.2 Spectral Method for Periodic Grids Scheme

First, a second-order FD scheme was written. Alternatively, we could take a fourth or sixth or higher-order scheme, which, of course, takes into account a larger number of grid points and will increase the rate of convergence of the numerical approximation. The idea of spectral methods is to take this process to the limit by interpolating the data globally [22]. There are several types of spectral methods for various problems; we chose the discrete Fourier transform because the phenomenon of interest in this project is unrelated to boundaries. The wave propagates at a maximum speed c, so we can approximate a suitable domain for the problem so that the disturbance, which is defined by a Gaussian, will vanish entirely at the edges. Taking the wave at the grid's boundaries to zero means we are dealing with a periodic grid. In spectral methods, a very useful, fast, and accurate method for periodic grids is the Fast Fourier Transform (FFT). This method enables us to compute the discrete Fourier transform of the domain points in $O(N \log N)$ floating points operations, and therefore the derivatives can be calculated by multiplying in the constant ik. The transforms are calculated by Matlab's programs 'fft' and 'ifft'. For the time derivative and the spatial derivative, we will use the finite difference and FFT, respectively.
By FD:

$$\frac{\varphi(x,t+\Delta t)-2\varphi(x,t)+\varphi(x,t-\Delta t)}{(\Delta t)^2} \approx \varphi_{tt}(x,t) = \varphi_{xx}(x,t) - \varphi(x,t) + F(x,x_p,t) \tag{3.9}$$

we will consider for every fixed x_j where $j = 1, ..., N$

$$\varphi_j(x_j,t) \xrightarrow[FFT]{} \hat{\varphi}_j(k,t) \tag{3.10}$$

Then multiply in Fourier space by $-k^2$ to get the second spatial derivative:

$$(\hat{\varphi_{xx}})_j = -k^2 \hat{\varphi}_j \tag{3.11}$$

And compute $(\varphi_{xx})_j$

$$(\hat{\varphi_{xx}})_j \xrightarrow[IFFT]{} (\varphi_{xx})_j \tag{3.12}$$

Finally, with this derivative we can update the future time term by (3.9):

$$\varphi_j(t+\Delta t) = (\Delta t)^2 (\varphi_{xx})_j (t) + \left(2-(\Delta t)^2\right) \varphi_j(t) - \varphi_j(t-\Delta t) + (\Delta t)^2 F_j(x_p,t) \tag{3.13}$$

For the equation of motion, the wave gradient will be calculated by interpolation of the derivative:

$$(\hat{\varphi}_x)_j = ik\hat{\varphi}_j \tag{3.14}$$

and $(\varphi_x)_j$ is:

$$(\hat{\varphi_x})_j \xrightarrow[IFFT]{} (\varphi_x)_j \tag{3.15}$$

at the location of the particle:

$$x_p(t+\Delta t) = x_p(t) - \alpha \frac{\partial \varphi}{\partial x}\Big|_{x_p(t)} \Delta t \tag{3.16}$$

It can be seen that by calculating the particle motion using the spectral method, we have already done part of the work by the Fourier transform in (3.10). In contrast, by using FD, the first derivative of the wave function had to be calculated at each time-step.

It should be noted that the spectral method doesn't have a symmetric grid, so a round-off error can lead to asymmetry even if no initial disturbance was given. Without any disturbance, the particle should be exactly centered in the middle of the time-changing Gaussian. Therefore, the gradient at the particle location is zero. Since the method is asymmetrical, a small size gradient slowly takes the particle out of symmetry. To overcome this problem, the gradient at the particle's point was rounded at the 10th decimal point to ensure that a gradient will not be created due to truncation error, and the method will remain symmetrical.

3.3 Sensitivity Tests for the Spectral Method

In order to test the convergence of the spectral method, the relative error of the average velocity of the particle, $\bar{v}$, was plotted as Δx and Δt decrease. Figure (3.1) (a) shows that the relative error $\eta(\Delta t)$ converge to 0 as the time step Δt decreases, for the different α values that were examined in this study. The error was tested for a fixed $\Delta x = 0.07$ and presented in a logarithmic scale. The convergence of the relative error of $\bar{v}$ as a function of the discretization of the spatial variable, $\eta(\Delta x)$, is represented in Figure (3.1) (b). The convergence was ensured for the same α values, as checked in Figure (3.1) (a), for a fixed time step value, $\Delta t = 10^{-3}$. From now on, we will use $\Delta t = 10^{-3}$ and $\Delta x = 0.07$, so the relative error is excepted to be less than 0.5%. An example of the particle trajectory, for $\alpha = 5$, and the influence of decreasing the spatial discretization is shown in Figure (3.2).

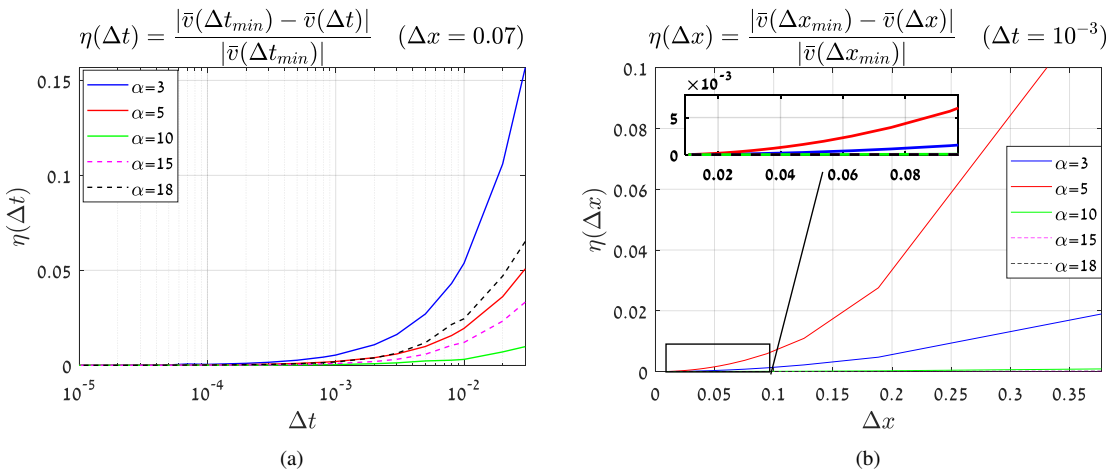

Figure 3.1: Convergence tests for the spectral method. The relative error η of the average velocity $\bar{v}$ of a particle trajectory as a function of (a) the temporal interval Δt and (b) the spatial interval Δx, for the range of α values that are examined in this project. For every Δt we took our final Δx of choice ($\Delta x = 0.07$) in (a) and in a similar way we chose a constant Δt step ($\Delta t = 10^{-3}$) for (b).

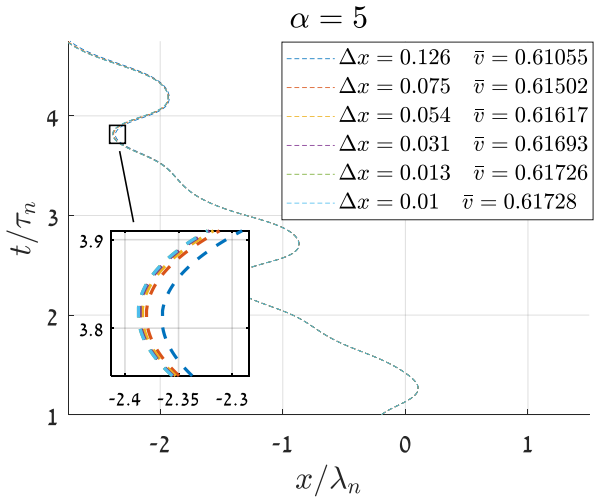

(a)

Figure 3.2: An example of the convergence of a particle trajectory while decreasing the spatial interval Δx, for $\alpha = 5$, and $\Delta t = 10^{-3}$. The particle trajectory convergence can be seen in the inset, and in the legend the tested variable, $\bar{v}$, converge to a final value.

3.4 Comparison between Finite Differences and the Spectral Method

The comparison between the numerical methods is divided into two parts: the first, only for the wave equation, and the second, the challenging computational part, for the coupled equations. First, we compared the methods only using the Klein-Gordon equation, with localized Gaussian as a periodic disturbance. As shown in Figure 3.3 (a), when it comes to just the wave equation without the dynamic coupling, the comparison is much better. After about $10\tau_n$, the maximum error between the waves is $6 \cdot 10^{-5}\lambda_n$. However, for the same initial condition, but this time with the dynamic coupling ($\alpha = 10$), as can be seen in Figure 3.3 (b), the maximum difference between the waves is $0.01\lambda_n$. This is also apparent in the difference between the particle trajectories in Figure 3.4, where the maximum difference is $0.05\lambda_n$. Nevertheless, for the order of $x = \lambda_n$, which is the scale of interest in this study, this discrepancy is negligible. The reason for the discrepancies created when adding the dynamic equation is the combination of small scales and large scales of the problem. The wave-field propagates at the maximum speed c, when the particle, at least in the beginning, is oscillating about the origin. As a result, the ratio between the particle's initial spatial location and the wave field is about ten thousand, which is computationally challenging, especially when trying to achieve both the accurate trajectory of the particle and the entire domain of the wave-field.

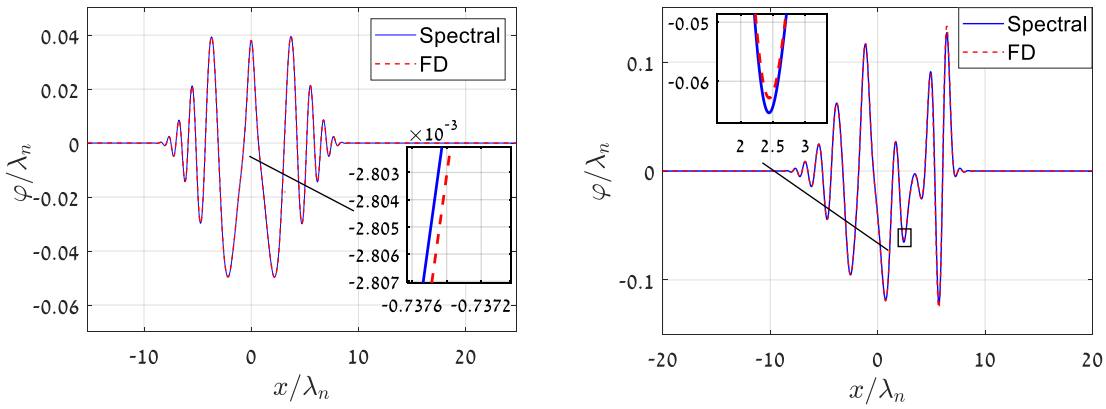

(a) (b)

Figure 3.3: Comparison between FD and FFT, with the same time and space intervals for both methods. (a) KG wave-form with a periodic Gaussian disturbance that is fixed in space. The maximum difference between the waves after $t = 10\tau_n$ is $6 \cdot 10^{-5}\lambda_n$. (b) The same comparison as in (a), but now for the coupled equations (the wave-KG equation and the dynamic equation for $\alpha = 10$), the maximum error is $0.01\lambda_n$.

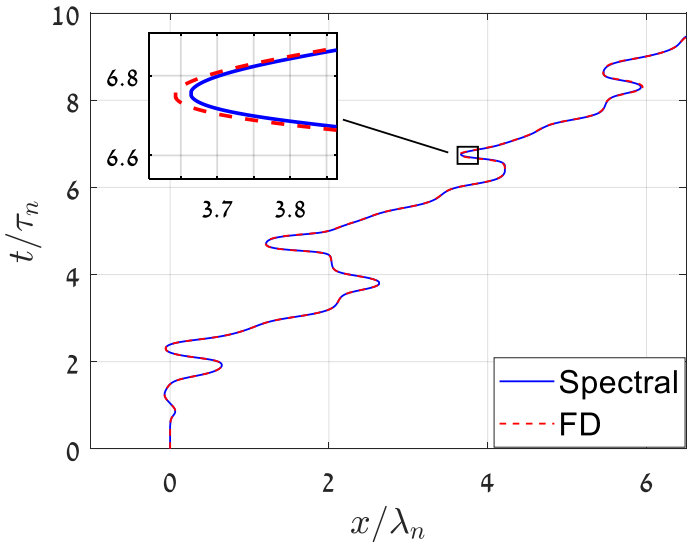

(a)

Figure 3.4: The particle trajectory comparison between the methods. The maximum error difference between the trajectories is $0.05\lambda_n$.

Chapter 4

Results and Discussion

4.1 Particle Dynamics and Wave-Form

The particle is free to move in space due to resonance interaction with the wave it creates. The simulations that will be presented in this section were conducted using the spectral method. To describes the fundamental problem, it is convenient to assume that the wave domain is $\mathbb{R}$, and the wave amplitude vanishes at infinity; but of course, for the simulation, finite boundaries must be defined. The wave propagates at a maximum speed c. This speed, together with the simulation time, determines the minimum size of the domain. In the simulation, we chose a domain three times larger than the maximum point the wave reaches. For all the cases examined in this study, the particle itself moves within the "light cone" - the spatiotemporal wave propagation region, so the influence of the domain's boundaries on the particle is negligible.

The particle generates a periodic disturbance in the shape of an oscillating Gaussian function centered at the particle location, which means that the particle should not move if everything is symmetric. This can be seen in Figure (4.1)(a,b). A small initial random wave perturbation is applied and starts the particle's motion, approximately four orders of magnitude smaller than the maximum wave amplitude, which is similar to the method suggested by Dagan and Bush [17] for HQFT simulations. The perturbation initially causes the particle to oscillate about its initial position (x = 0) with a small amplitude. Later, depending on α, the constant that determines how strongly the wave slope affects the particle velocity (the influence of that constant will be discussed later), the symmetry breaks, the oscillations are wider, and the particle is easily deflected. At this point, the particle motion is highly sensitive to the initial perturbation. In this part of the motion, the particle's direction is determined in which it will persist. This transition seems to have chaotic characteristics. The time at which the symmetry in the particle's motion is broken increases as α decreases (Figure (4.1) (c) compared to Figure (4.2) (a) and (c)).

There are several forms of the transition part of the motion. Two examples for these different particle dynamics are shown in Figure (4.1), one with direction change of the particle even after breaking the symmetry Figure (4.1) (c), and the other with a straight attachment to constant motion in one direction Figure (4.1) (d).

A fascinating feature that can be seen in the results, which emphasizes the wave-particle interaction compared to quantum mechanics, is the connection between the wavenumber or the wavelength to the particle's momentum. At the beginning of the motion, next to the particle, the wave has a large wavelength (Figure (4.2) (b)). However, after the motion is locked into constant average velocity, the wavelength is much smaller (Figure (4.2) (d)). This can be understood by presenting de Broglie's relation between the momentum and the wavenumber in QM: $p = \hbar k$.

In the first part of motion, the particle is drifting slowly (Figure (4.2) (d) for $t \in [0, 15]\tau_n$), and the wave number is small (the wavelength is large). This can be seen more drastically in Figure (4.1)(b), where the particle doesn't move at all, and the wavenumber goes to 0. In the second part, the average velocity of the particle reaches the peak velocity and therefor k and the particle momentum p is the greatest, as in Figure (4.2) (d) and further increases in Figure (4.3), where the particle average velocity is almost c. It is important to mention that the particle's velocity

in this project passes the speed c. However, the interest is on the average velocity, the drift speed, which notably does not exceed the speed c in any of the cases investigated here. Moreover, the particle's momentary high-speed is oscillating at a characteristic length of λ_n about the average. After some deflections that change the trajectory dramatically, the particle locks into a constant speed on average less than c, and it will persist in its state; the size of this quasi-steady motion velocity will be discussed in the next section.

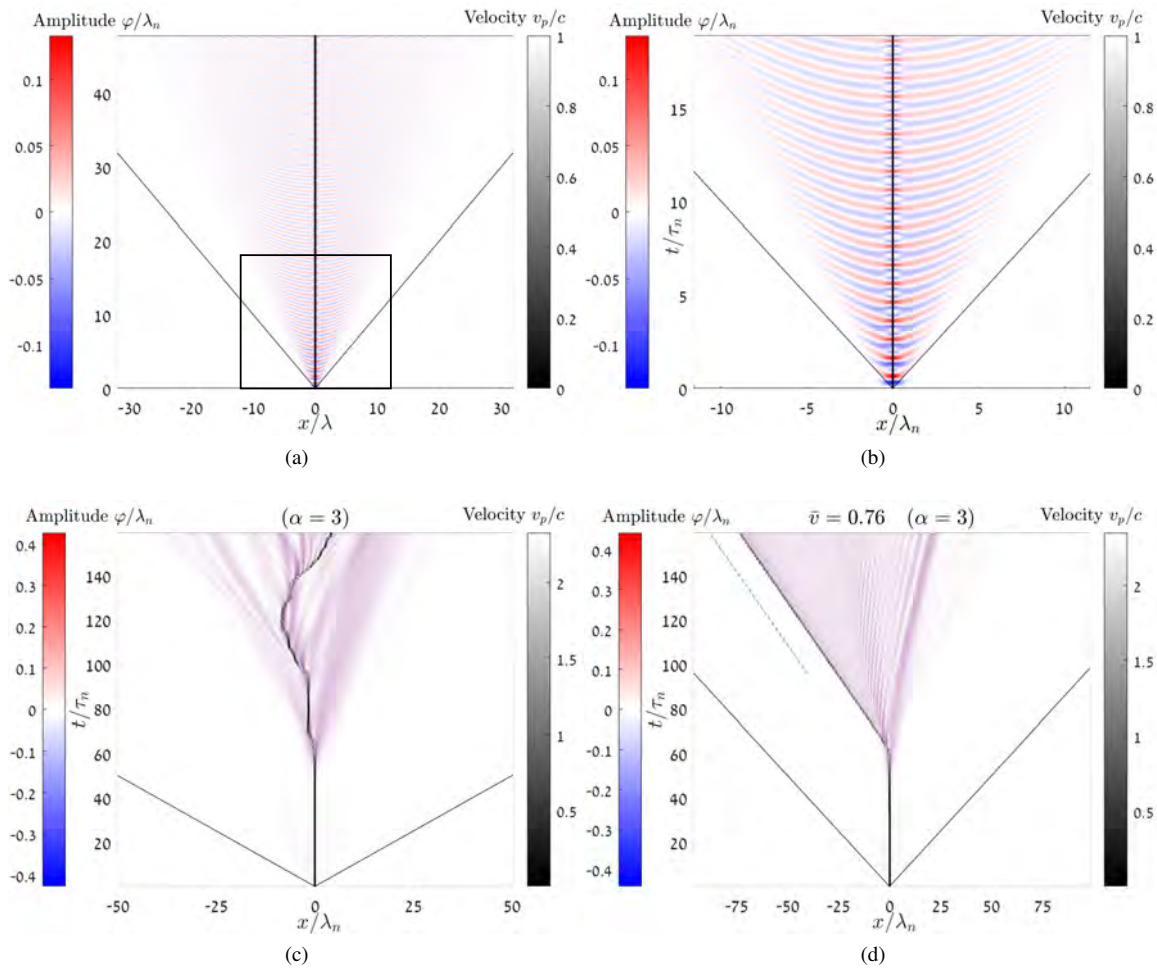

Figure 4.1: Spatio-Temporal map, showing the connection between the particle location and the wave amplitude as a function of time. The trajectory is color-coded by the particle speed v_p. Without an initial perturbation (a,b), for a coupling parameter $\alpha = 3$, the particle is located at the top of the Gaussian, where the gradient is zero, so the particle is static and located in $x = 0$. Small initial random wave perturbation is applied, and at (c,d) for the same coupling parameter, the particle is self-propelled. (c,d) are two examples for different particle dynamics, one with direction changes even after breaking the symmetry (c), and the other with a straight attachment to constant motion in one direction (d).

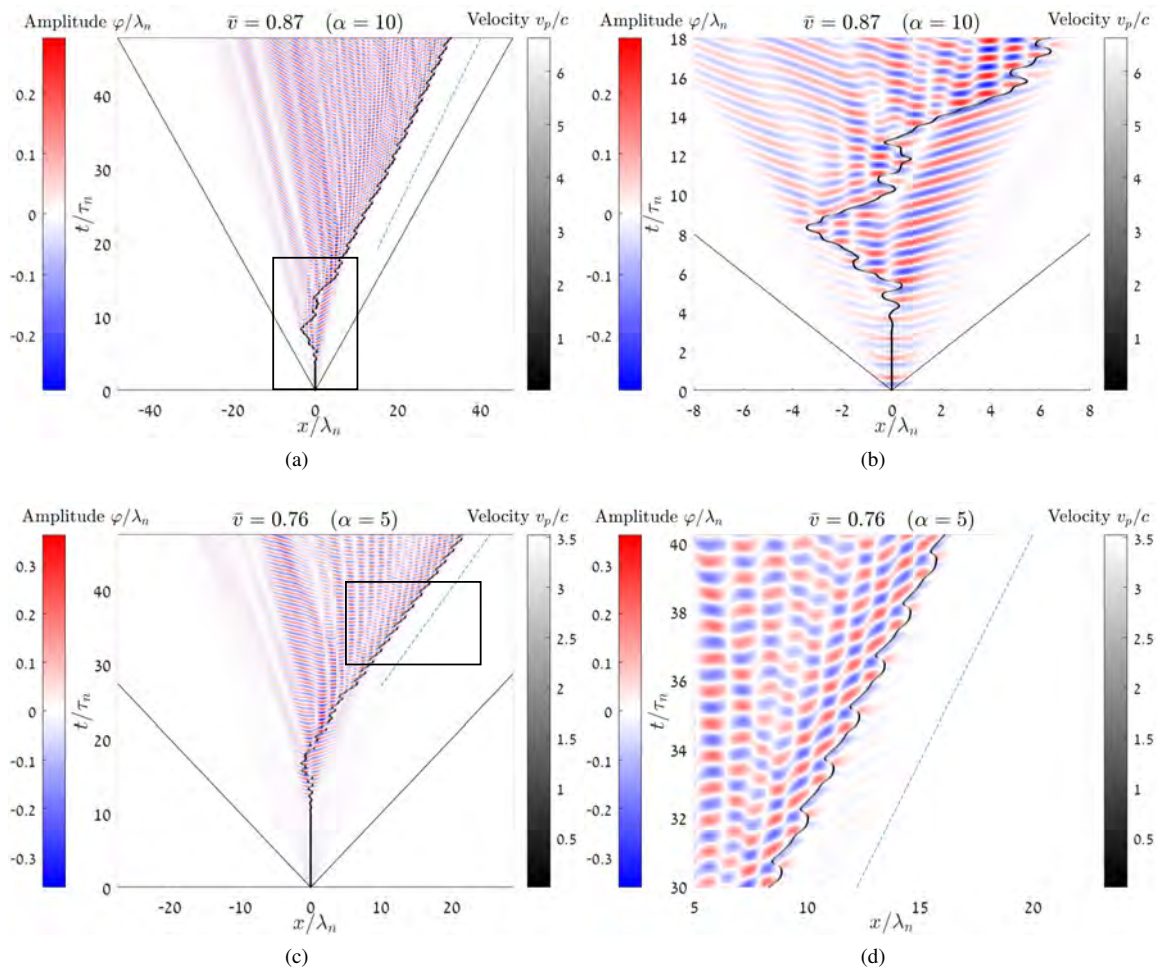

Figure 4.2: Spatio-Temporal map, showing the connection between the particle location and the wave amplitude as a function of time. The trajectory is color-coded by the particle speed v_p. Small initial random wave perturbation is applied. Insets showing zoom-in plots in (b) and (d) of different trajectories for different sizes of $\alpha = 5, 10$. At the first part of the motion, the particle is drifting slowly (b), and the wave number is small; in the second part, the particle's average velocity reaches the peak velocity and therefore k and the particle momentum p is the greatest (d).

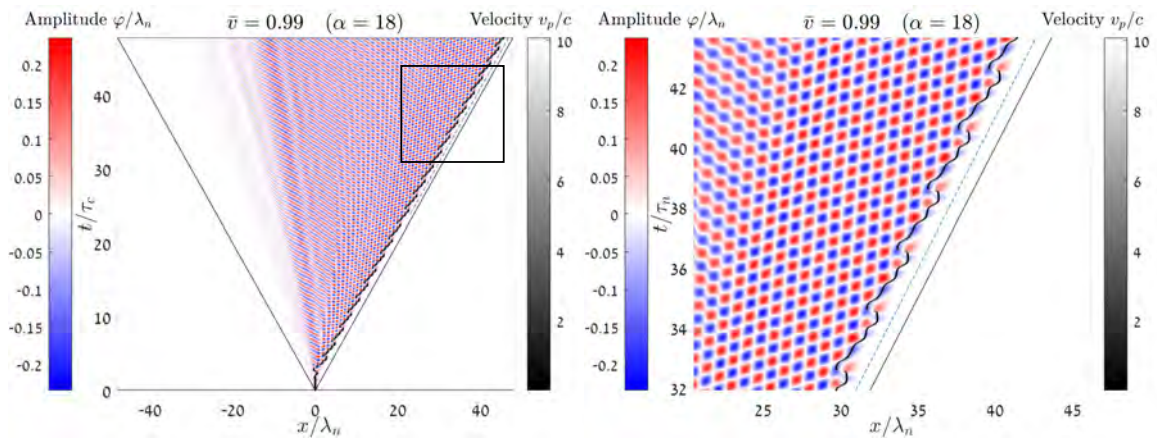

(a) (b)

Figure 4.3: Spatio-Temporal map, showing the connection between the particle location and the wave amplitude as a function of time. The trajectory is color-coded by the particle speed v_p. Small initial random wave perturbation is applied. Inset showing zoom-in plot (b) for largest coupling parameter in this study, $\alpha = 18$. The trajectory is characterized by an almost immediate attachment to constant motion in one direction, and the particle travels close to the speed c, but does not pass it on average.

4.2 Particle Statistics and Typical Properties

In order to better understand the properties of the particle's motion, such as the typical time for symmetry breaking, characteristic average velocity, and the temporal evolution of the trajectories, 80 simulations of particle trajectories for different values of α were run (Figure (4.4) (a),(b)). Each of the simulations for the same α was initiated with identical conditions except for the random initial perturbation. These simulations help to understand the influence of α, the coupling coefficient that multiplies the wave gradient term in the particle's dynamic equation (2.15).
We define the time of breaking the symmetry as the time at which the particle exits the range $x \in [-\lambda_n/2, \lambda_n/2]$. In Figure (4.4) (c), we present the normalized breakup time t_b/τ_n as a function of α, and we can assume that:

$$\begin{cases} t_b/\tau_n \longrightarrow 0 & \text{for } \alpha \longrightarrow \infty \\ t_b/\tau_n \longrightarrow \infty & \text{for } \alpha \longrightarrow 0 \end{cases} \tag{4.1}$$

Moreover, as α increases, the particle is more influenced by the wave gradient, the trajectories are more centered around the average value, and the standard deviation-error bar is smaller. Similarly, as α grows, the particle's average velocity increases and the standard deviation is smaller Figure (4.4) (d). These two phenomena can be distinguished from the trajectory plots for different values of α in Figure (4.4) (a),(b). In (a), one can see a variety of colors that present the velocity, suggesting the particle has a wide range of speeds relative to the maximum velocity of its motion. The group of trajectories on each side is wide, and several particles change the direction of their persistence, even after leaving symmetry. On the other hand, In (b), the primary color is blue; the velocities are low relative to their maximum speed. Most of the trajectories seem similar, and the spread of trajectories is narrow.

One explanation for this behavior is the inherent relativistic essence of the KG equation. The particle oscillations generate the waves and drifting motion. This form of dynamics occurs because the wave-field carries the particle from different sides of the wave's peaks, while the gradient's sign at the location of the particle changes over time. These gradient oscillations attenuate the particle's velocity, and even though the particle's momentary velocity is

very high, the mean motion is much slower. The group velocity is the velocity at which information is conveyed along a wave, and for KG is:

$$C(k) = \frac{d\omega(k)}{dk} = \frac{c^2 k}{\sqrt{{\omega_c}^2 + c^2 k^2}} \tag{4.2}$$

This speed is always smaller than c; the wave thus carries the particle in a way that alters the particle's high-velocity dynamics due to large α and limits it, so it does not pass the speed c.

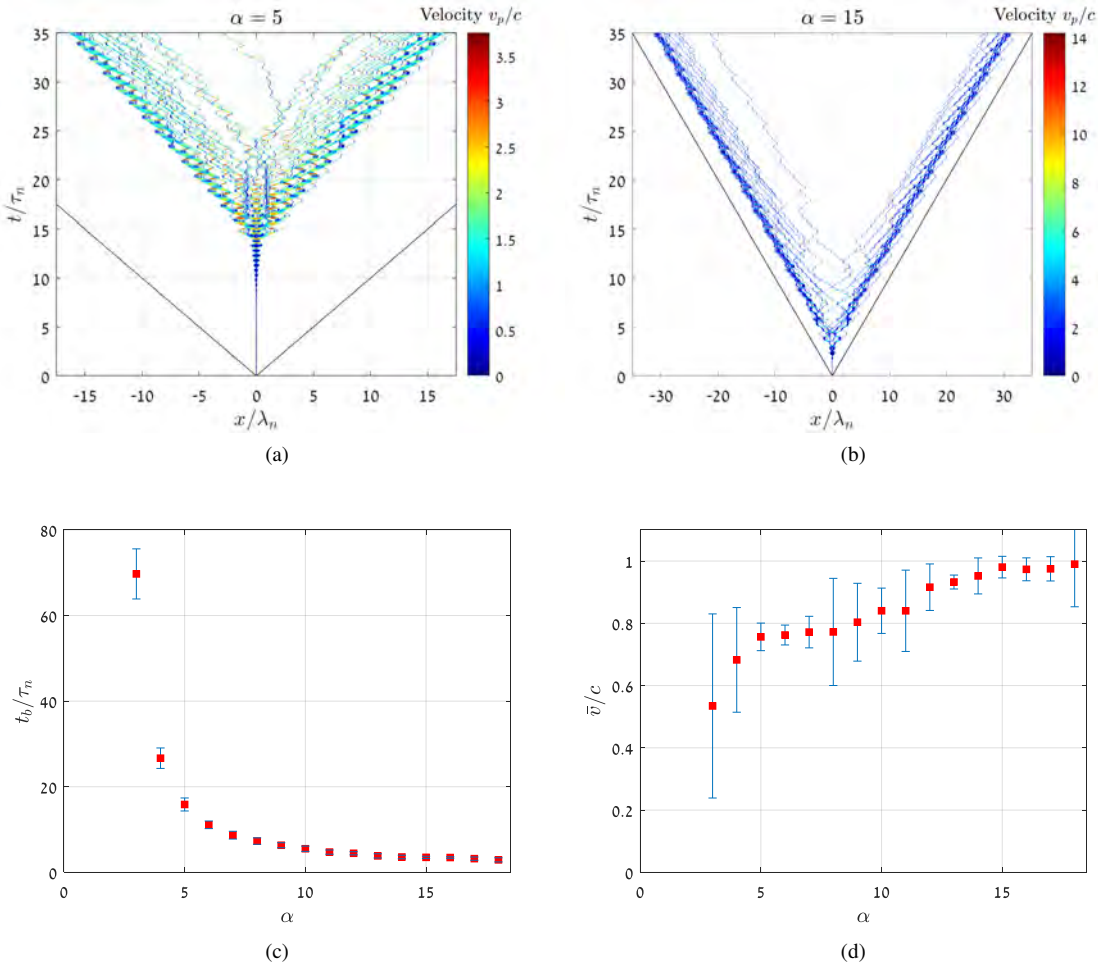

Figure 4.4: Statistics and typical properties of the particle motion. (a) 80 simulations for $\alpha = 5$, and (b) $\alpha = 15$. Each one of the simulations for the same α has identical conditions except for the random initial perturbation. (a,b) are examples of the simulation trajectories and each plot presents the location of the particle as a function of time, color-coded by the velocity of the particle relative to the maximum velocity of the 80 simulations. (c) The time of breaking the symmetry, at which the particle exits the range $x \in [-\lambda_n/2, \lambda_n/2]$. (d) The average velocity of the particles in the region of quasi-steady motion. In (c,d), the blue error bars represent each simulation's standard deviation. As α increases, the standard deviation decreases, and $\bar{v}$ increases.

Chapter 5

Conclusions and Future Research

In this research, we investigated a new pilot-wave theory, recently developed by Dagan and Bush [17], which proposes two coupled equations to explain as simply as possible the dynamics behind the pilot-wave theory for both bouncing droplets and free particles in quantum mechanics. In contrast to their study, in this project, we relaxed the assumption that relativistic dynamics govern the particle motion, and the dynamic equation is suitable for non-relativistic fluid dynamics and is not restricted by special relativity.

We developed a new spectral method to solve the coupled equations, verified the method's convergence, and validated this method with a Finite Difference method that was also written here.

There is a considerable variation in the scales between the particle motion and the wave-field, which makes it a challenge to compute the solution of the coupled equations for such sensitive particle oscillations in an appropriate domain.

In the results and discussion section, we characterized the particle's self-excitation of motion for small initial perturbations. It can be seen in different parts of the motion that there is a direct correlation between the wavelength, and the particle's velocity, as expected in QM, by the relation $p = \hbar k$.

The statistics for different values of α were collected to describe the particle's relativistic behavior. In this new model, we suggested that a relativistic dynamic equation as in [17] may not be required in order to achieve quantum-like statistics and even relativistic behavior for time scales larger than τ.

For all cases considered in this project, increasing α had increased the inline-oscillation velocity, but the averaged velocity did not exceed c.

In the future, we would like to check what be the effect on the trajectory if we change the thickness of the periodic Gaussian disturbance. We will try to reduce this width and examine the influence of both α and the width-a on the motion.

We will also try to compare this theory to an experiment, using the coupled equations to represent the droplet's motion. Hopefully, using additional potentials and other forces, we will employ this theory to describe phenomena that occur both in the quantum world and in the pilot-wave droplets system.

Bibliography

[1] Yves Couder et al. "Walking and orbiting droplets". In: *Nature* 437.7056 (2005), pp. 208–208.

[2] Suzie Protiere, Arezki Boudaoud, and Yves Couder. "Particle-wave association on a fluid interface". In: *Journal of Fluid Mechanics* 554 (2006), p. 85.

[3] John WM Bush. "Pilot-wave hydrodynamics". In: *Annual Review of Fluid Mechanics* 47 (2015), pp. 269–292.

[4] John WM Bush. "The new wave of pilot-wave theory". In: (2015).

[5] Yves Couder and Emmanuel Fort. "Single-particle diffraction and interference at a macroscopic scale". In: *Physical review letters* 97.15 (2006), p. 154101.

[6] A Eddi et al. "Unpredictable tunneling of a classical wave-particle association". In: *Physical review letters* 102.24 (2009), p. 240401.

[7] André Nachbin, Paul A Milewski, and John WM Bush. "Tunneling with a hydrodynamic pilot-wave model". In: *Physical Review Fluids* 2.3 (2017), p. 034801.

[8] Maxime Hubert, Matthieu Labousse, and Stéphane Perrard. "Self-propulsion and crossing statistics under random initial conditions". In: *Physical Review E* 95.6 (2017), p. 062607.

[9] Emmanuel Fort et al. "Path-memory induced quantization of classical orbits". In: *Proceedings of the National Academy of Sciences* 107.41 (2010), pp. 17515–17520.

[10] Daniel M Harris and John WM Bush. "Droplets walking in a rotating frame: from quantized orbits to multimodal statistics". In: *Journal of fluid mechanics* 739 (2014), p. 444.

[11] Anand U Oza et al. "Pilot-wave dynamics in a rotating frame: on the emergence of orbital quantization". In: *Journal of fluid mechanics* 744 (2014), pp. 404–429.

[12] A Eddi et al. "Level splitting at macroscopic scale". In: *Physical review letters* 108.26 (2012), p. 264503.

[13] Tudor Cristea-Platon. "Hydrodynamic analogues of quantum corrals and Friedel oscillations". PhD thesis. Massachusetts Institute of Technology, 2019.

[14] Pedro J Sáenz, Tudor Cristea-Platon, and John WM Bush. "A hydrodynamic analog of Friedel oscillations". In: *Science Advances* 6.20 (2020), eaay9234.

[15] Daniel M Harris et al. "Wavelike statistics from pilot-wave dynamics in a circular corral". In: *Physical Review E* 88.1 (2013), p. 011001.

[16] Pedro J Sáenz, Tudor Cristea-Platon, and John WM Bush. "Statistical projection effects in a hydrodynamic pilot-wave system". In: *Nature Physics* 14.3 (2018), pp. 315–319.

[17] Yuval Dagan and John WM Bush. "Hydrodynamic quantum field theory: the free particle". In: *Comptes Rendus. Mécanique* 348.6-7 (2020), pp. 555–571.

[18] Matthew Durey and John WM Bush. "Hydrodynamic quantum field theory: the onset of particle motion and the form of the pilot wave". In: *Front. Phys* 8 (2020), p. 300.

[19] Franz Gross. *Relativistic quantum mechanics and field theory*. John Wiley & Sons, 2008.

[20] Øistein Wind-Willassen et al. "Exotic states of bouncing and walking droplets". In: *Physics of Fluids* 25.8 (2013), p. 082002.

[21] Anand U Oza, Rodolfo R Rosales, and John WM Bush. "A trajectory equation for walking droplets: hydrodynamic pilot-wave theory". In: *Journal of Fluid Mechanics* 737 (2013), pp. 552–570.

[22] Lloyd N Trefethen. *Spectral methods in MATLAB*. SIAM, 2000.